Hindawi Publishing Corporation
Advances in Meteorology
Volume 2014, Article ID 783718, 9 pages
http://dx.doi.org/10.1155/2014/783718

Research Article

Forecasting Hydrological Disaster Using Environmental Thermographic Modeling

Moses E. Emetere

Department of Physics, Covenant University, Canaan Land, PMB 1023, Ota, Nigeria

Correspondence should be addressed to Moses E. Emetere; emetere@yahoo.com

Received 11 May 2014; Accepted 2 July 2014; Published 12 August 2014

Academic Editor: Sven-Erik Gryning

The concept of thermographic model is new to environmental studies. Its mode of operation is fairly synonymous to the operational technique of the regular thermography machine. The location of the study area is between latitudes 8°24′N and 9°20′N of the equator and between longitudes 7°30′E and 8°48′E of the Greenwich Meridian. The subsoil for the soil samples was identified within the particles range 63 ± 3% sand, 28 ± 5% clay, 6 ± 2% silt, 0.9 ± 0.3% organic carbon, and 1 ± 0.2% organic matter. Field work was carried out and the measurements obtained were validated using satellite data. At shallow ground depth, the thermal diffusivity is not proportional to either the increase or the decrease in the ground temperatures. Features of the temperature anomaly showed strange shifts per month within 2012. The environmental thermographic model (ETM) can be adopted by meteorological ground stations to investigate the net radiation over the land. The ability of the ETM could be extended to monitoring ground anomalies like fractures of basic rocks amongst others.

1. Introduction

The use of environmental thermographic model (ETM) is quite rare in environmental studies. ETM has a thermographic plate (earth) which accounts for both activities above and below the earth surface. One key parameter of the ETM is the ground temperature. Ground temperature is categorized as one of the notable variables of land surface climatology. It is greatly influenced by the longwave and shortwave radiation. Ground temperature is dependent on different soil variables/parameters, for example, soil properties and soil compaction [1, 2]. Several models had been used to discuss the dimensions of ground temperature. One of such models is the empirical and mechanistic model. This model had been successful in predicting ground temperature using soil depth and heat flow principles [3], relating ground temperatures to climatology change [4] and relating ground temperature to soil depth and variables [5, 6]. Significantly, scientists [7–9] have been able to show that ground temperature can be generated from some salient factors which include air temperature, humidity, and longwave and shortwave radiation. In other words, ground temperature is determined by energies from net radiation, latent heat flux, sensible heat flux, and soil heat flux. Recently, Uno and Emetere [10] related the soil heat flux, sensible heat flux, and net radiation to the ground temperatures. A polynomial scheme known as the temperature polynomial expansion scheme (TPES) was propounded to show that the net radiation had greater influence on the ground temperatures. Though the net earth radiation and the ground temperature are directly proportional to one another, measurements of the ground temperature are very necessary for the understanding of biological, hydrological, and climatological systems [11, 12]. In measuring accurately the ground temperature, renown methods were used, for example, air borne radiometer [13, 14] and satellite sensors [11, 15–18]. Ground temperatures have been related to geothermal data [19]. This explains why the earth behaves as a low-pass filter recording long-term trends of ground surface temperature changes [20].

In this paper, we propose that the top ground layer of the earth acts like a thermographic film. Therefore in this study, the thermographic film or plate is referred to the top ground layer of the earth. The thermographic film depends on some salient parameters, for example, the soil formation of an area, the magnitude of longwave and shortwave radiation, and so forth. For example, the study area in this paper is

underlain by crystalline basement complex rocks. Soil in areas of crystalline basement complex rocks is characterized by high thermal absorption. We believe that this kind of thermographic film would allow all the environmental forces, for example, air temperature, solar irradiance, and precipitation patterns, to inscribe their effects on the overall ground temperature data at specific time of the year. The objective of this paper is to introduce the ETM in a simple way by the observance of its key parameter (ground temperature). We believe that the application of ETM is not limited to only meteorological predictions, but it extends to geological studies.

2. Theory

Ingersoll et al. (1954) formulated an equation from the diffusion of heat equation for a semi-infinite solid. This equation relates ground temperature at a given depth to time as shown below:

$$T(z,t) = \frac{1}{2}T(0)\exp -z\left(\frac{\pi}{\alpha P}\right)^2 \sin\left[\frac{2\pi t}{p} + \emptyset(z)\right] + T_m, \quad (1)$$

where $T(z,t)$ is the temperature (°c) z centimeters below the surface at a time t, $T(0)$ is the peak-to-peak temperature variation at the surface (°c), z is the depth below the surface, t is the time, α is the thermal diffusivity of the material, P is the period of the wave, $\emptyset(z)$ is the phase of the wave at a depth z below the surface, and T_m is the mean annual temperature.

Hillel [21] also gave the annual variation of daily average soil temperature at different depths with a sinusoidal function. Consider

$$T(z,t) = T_a + A_0 e^{-z/d} \sin\left(\frac{2\pi(t - t_o)}{365} - \frac{z}{d} - \frac{\pi}{2}\right), \quad (2)$$

where $T(z,t)$ is the soil temperature at time (t), z is the soil depth, T_a is the average soil temperature (°C), A_0 is the annual amplitude of the surface soil temperature (°C), d is the damping depth (m) of annual fluctuation, and t_0 is the time lag.

Uno et al. [22, 23] derived the temperature deviation curve model. Basically, it is represented as

$$\Delta T = A_0 e^{-\rho_s/\rho_b} \sin\left(-\frac{\rho_s}{\rho_b} - \frac{\pi}{2}\right), \quad (3)$$

where ρ_s = soil particle density which is approximately 2.66 gcm^{-3} by Gupta et al. [3], ρ_b = soil bulk density. It was used to determine the susceptibility of Abuja metropolis to soil compaction [10], determine the annual amplitude of the surface soil temperatures of the same region [10], estimate soil heat flux from both short-term and long-term remotely sensed surface temperature [22], and estimate earthquake impact [24].

From (1) and (2), we made an assumption that the heat flux is distributed evenly over the covered surface; that is, the sine waves are equal, $\emptyset(z) = -(z/d) - (\pi/2)$, and the peak-to-peak temperature vanishes; that is, $(1/2)T(0) = 1$. The resulting equation is as follows:

$$\Delta T = e^{-z(\pi/\alpha)^2} \sin\left[\frac{2\pi(t - t_o)}{365} + \emptyset(z)\right], \quad (4)$$

where $\Delta T = T(z,t) - T_m$.

3. Material and Method

The study area is Abuja, Federal Capital Territory (FCT), northern-central region of Nigeria. The soil samples were collected from the sampling sites in Kubwa-Bwari area council (Figure 1).

The region of study is located between latitudes 8°24′N and 9°20′N of the equator and between longitudes 7°30′E and 8°48′E of the Greenwich Meridian. The study was carried out at 30 cm soil depth. The subsoil for the soil samples was identified within the particles range 63±3% sand, 28±5% clay, 6 ± 2% silt, 0.9 ± 0.3% organic carbon, and 1 ± 0.2% organic matter. Kubwa is located within the Bwari area council and its environs are mostly residential. Drenches were made on the study site. Six thermometers were inserted at exactly 30 cm below the soil surface as shown in the prototype in Figure 2.

The thermometers were spaced five (5) metres apart along each drench. The drench was properly covered using wood (i.e., plank) and a black polythene bag. The thermometers were read and recorded hourly, that is, 11am and 2pm at the peak solar radiation for each day. The average readings were recorded as against each day. The experiment duration was twelve (12) months. The ground temperature was harvested and analysed by the ETM. The study area is underlain by crystalline basement complex rocks as shown in the geological map in Figure 3.

4. Results and Discussion

Our first objective is to create a standard theoretical control for the study area. The graphical representation of (4) is shown in Figure 4 under the condition that $-z(\pi/\alpha)^2 = 0.85$ and the wave phase varies proportionally to the days of the month.

$-z(\pi/\alpha)^2 = 0.85$ was derived from the experimental results as shown in Figure 5. The average positive minimum value (within the year) of ΔT from Figure 5 is given as 0.51 K, while the angle $\theta = (2\pi(t - t_o)/365) + \emptyset(z)$ was derived from the triangle ABC whose height $\overline{\mathrm{AB}}$ cuts across the extremes of ΔT (see Figure 5).

The sinusoidal graph (where the x-axis and y-axis are "days of the month" and "deviation ground temperature," resp.) illustrates an ideal case ground temperature variations during the year (see Figure 4). The experimental values for the year are shown graphically in Figure 5.

The positive and negative peaks show different characteristic feature trapped by the thermographic plate/film. This feature is traceable to the total earth's net radiation [23]. In the first hundred and ten (110) days of the year (see Figure 5), there was rarefaction with considerable size-signifying excessive heating of the land mass. At this point, the ground temperatures experience an almost uniform increase and decrease in ground temperatures. The compression within the 110–180 days (see Figure 5) shows that the thermographic film/plate responds to different doses of solar radiation. At this particular period of the year, the study area experienced flooding. This implies that, when there is a sharp compression in the ground temperatures as shown in Figure 5, disaster

Table 1: Inconsistent relation between ground temperature and thermal diffusivity.

Thermal diffusivity (m^2/s)	9.97	7.02	5.33	2.75	2.75	2.75	1.60	4.01	2.44
Temperature (°C)	27.10	27.20	27.00	26.40	26.40	26.40	27.60	28.40	29.20

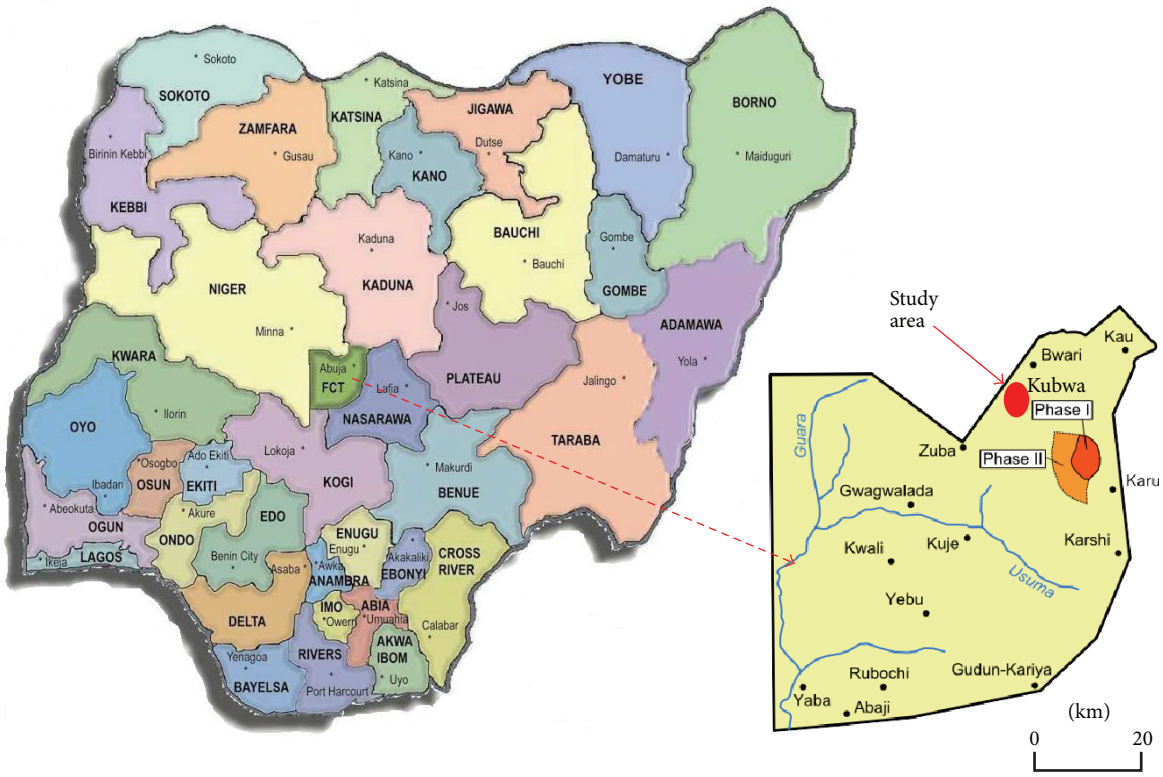

Figure 1: The geographical map of study area.

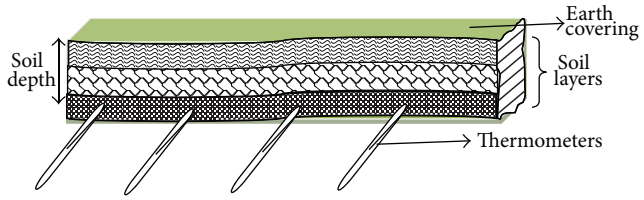

Figure 2: Practical measuring method for determining ground temperature.

may be imminent over such area. The other shapes of the graph beyond the hundred and eighty days (180) are sinusoidal (as expected by theoretical predictions (Figure 4)) and more stable (Figure 5). The downward trend of the graph in the last few days of the year shows that there may be a turning point upwards by January 2013. The implication of this hypothesis is that since higher ground temperature is a result of a higher dose of solar radiation over the thermographic film/plate, higher solar radiation is expected for January 2013. This assertion has been confirmed by NASA satellite imagery. Therefore, we propose that the ETM is a good tool for meteorological application. Closer analyses were carried out on a monthly basis (January to December in Figures 6–17) to express the various features of the earth's net radiational capture and its likely interpretations for future hydrological forecast. The regular sinusoidal line represents the theoretical prediction which is assumed to be uniform throughout the year. The irregular sinusoidal line is the experimental traces of the ground temperatures for the month. The dotted/dashed line represents the radiational pattern of the earth's net radiation over the thermographic film/plate.

The ground temperature for the month of January (as shown in Figure 6) had a peculiar pattern. The temperature deviation from its mean ground temperature was parabolic graph (see the dotted lines) whose order can be written mathematically as $y = ax^n - bx \pm c$, where $0 \geq x \geq 31$. Here, "y" is the ground temperature deviation and "x" is the number of wavelength within the year. The thermal diffusivity (obtained from the nine points of intersection between the theoretical and experimental values) was discovered to be largely dependent on the soil properties and independent of neither the ground temperature nor net radiation as shown in Table 1. This discovery was consistent throughout the year. In February, the ground temperature deviated with respect to its mean temperature as calculated from the raw data (Figure 7). It showed two sharp positive and negative curves (see the dotted lines). It affirmed the solar radiation fluctuations within the month.

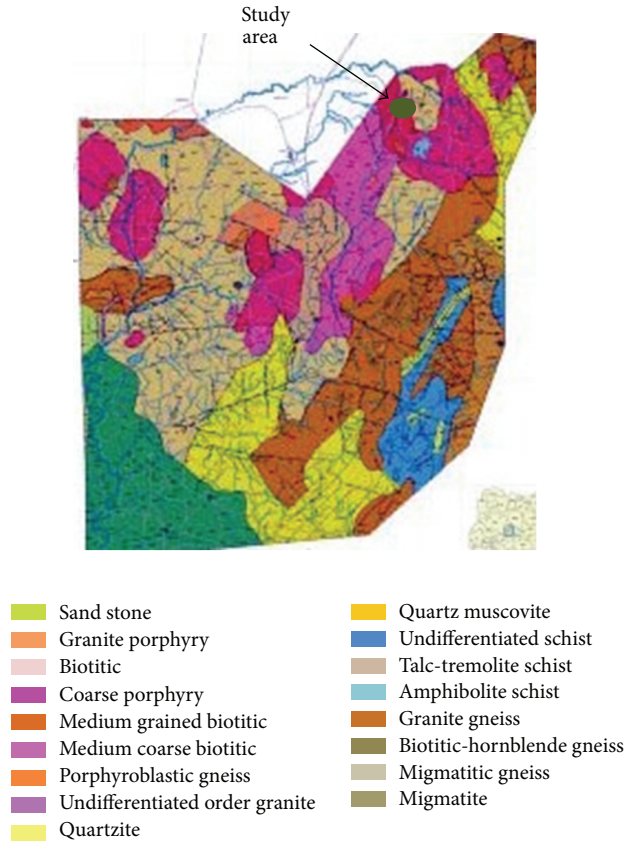

Figure 3: The geological map of study area.

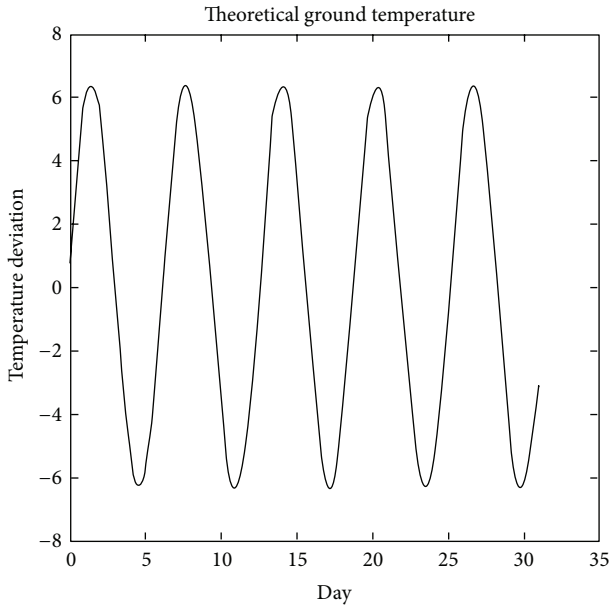

Figure 4: Theoretical analysis when $-z(\pi/\alpha)^2 = 0.85$.

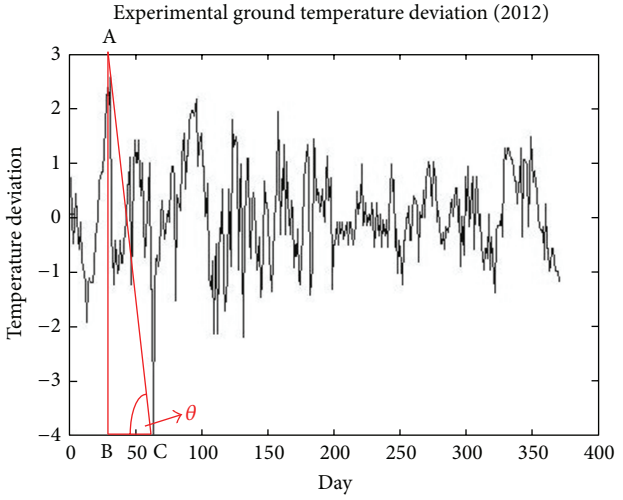

Figure 5: Experimental data for one year (2012).

In March, the ground temperature deviated with respect to its mean temperature for the month (Figure 8). It showed a linear relationship (see the dotted lines). This also showed the relative build-up of the solar radiation over the region within the month which is normal for the tropical region. In April, the ground temperature deviated with respect to its mean temperature (Figure 9) showing a negative curve. The solar radiation drops initially and then picks up slowly (see Figure 9).

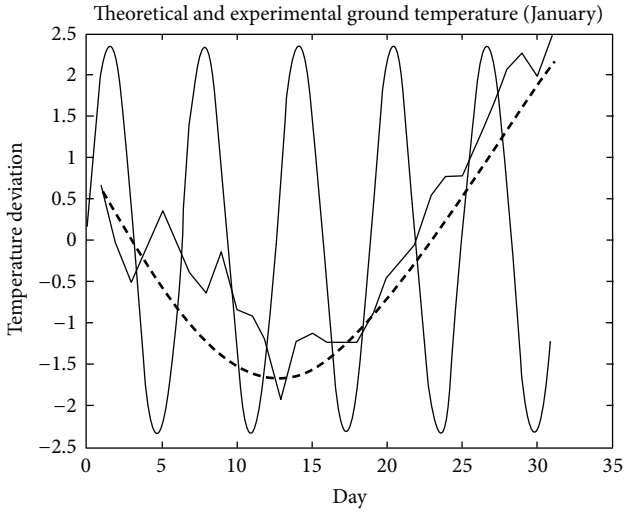

Figure 6: Theoretical and experimental combination for January.

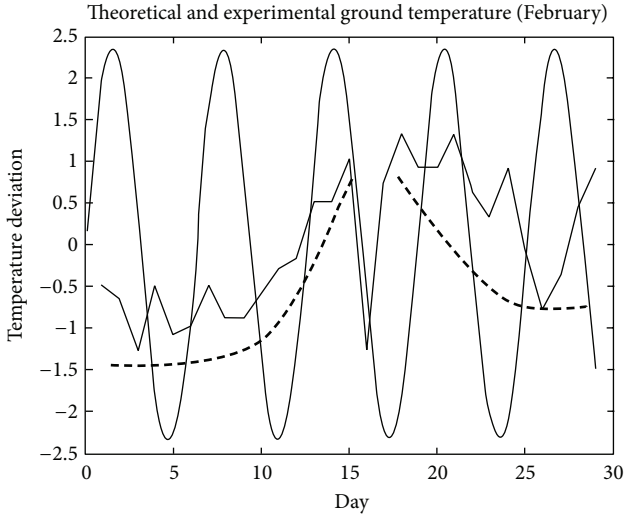

Figure 7: Theoretical and experimental combination for February.

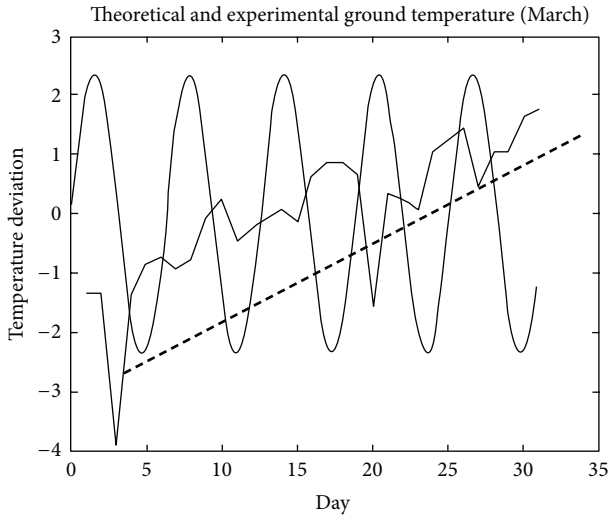

Figure 8: Theoretical and experimental combination for March.

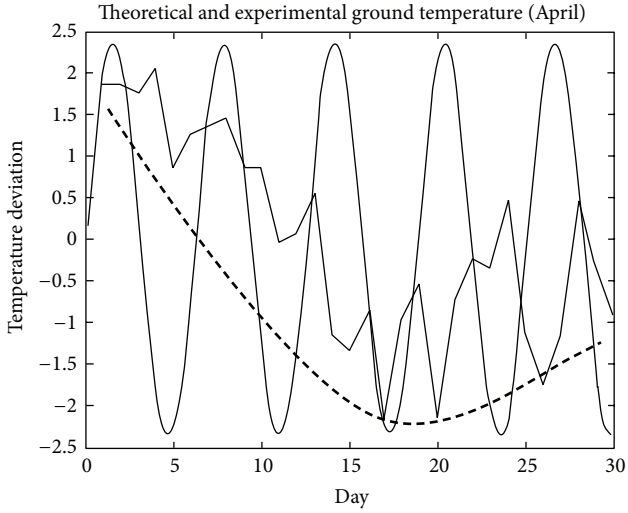

Figure 9: Theoretical and experimental combination for April.

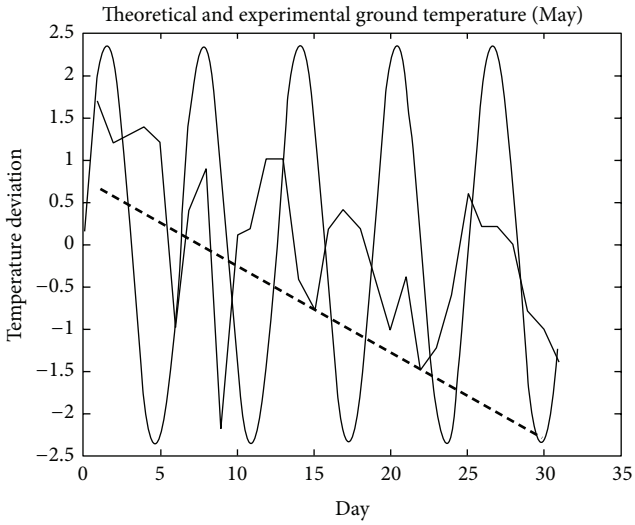

Figure 10: Theoretical and experimental combination for May.

The months of May and June showed the same ground temperature pattern (see Figures 10 and 11), that is, a gradual decrease of the solar radiation. Unfortunately, this period was the peak of flooding with higher magnitudes along the river rime and valley-like regions of the study area. Though this period was characterized with high rainfall, it was still abnormal for the ground temperatures (with respect to their mean temperature for the month) to keep dropping.

In July, the ground temperature deviated with respect to its mean temperature for the month (Figure 12). It showed a stable solar radiation and absorption as predicted theoretically. Nevertheless, the parallel downward shift suggests a stable drop of solar radiation (see dotted lines). August had the almost perfect stable solar radiation and absorption (Figure 13) as predicted theoretically.

The month of September witnessed a gradual positive increase of the deviated ground temperature like in the month

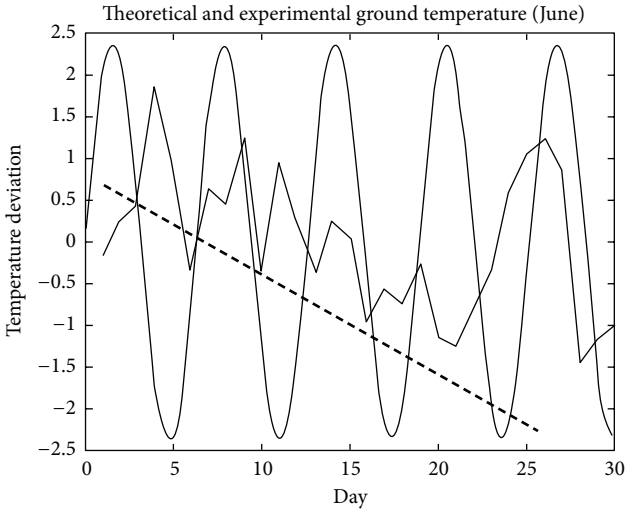

Figure 11: Theoretical & experimental combination for June.

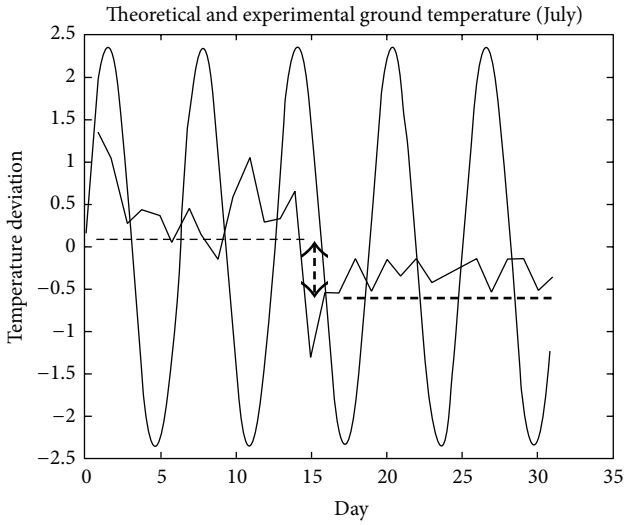

Figure 12: Theoretical & experimental combination for July.

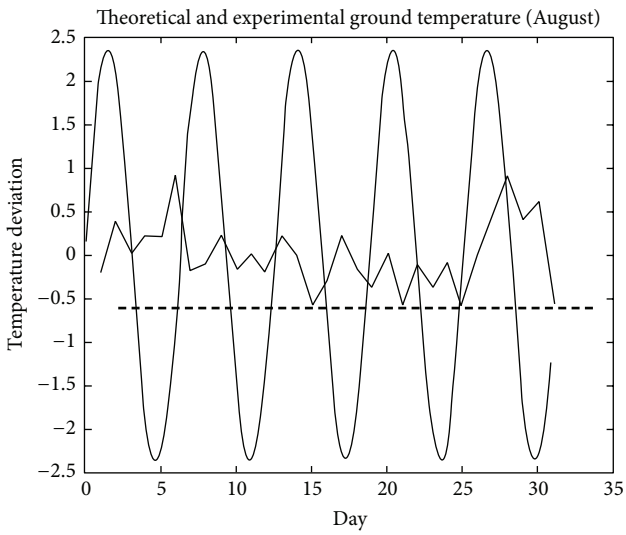

Figure 13: Theoretical & experimental combination for August.

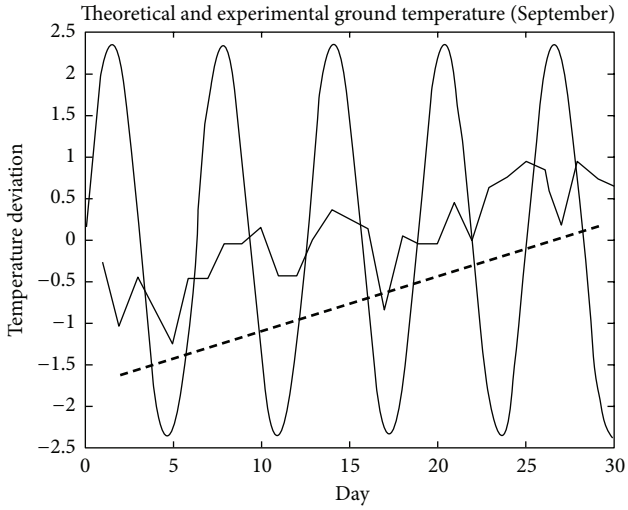

Figure 14: Theoretical and experimental combination for September.

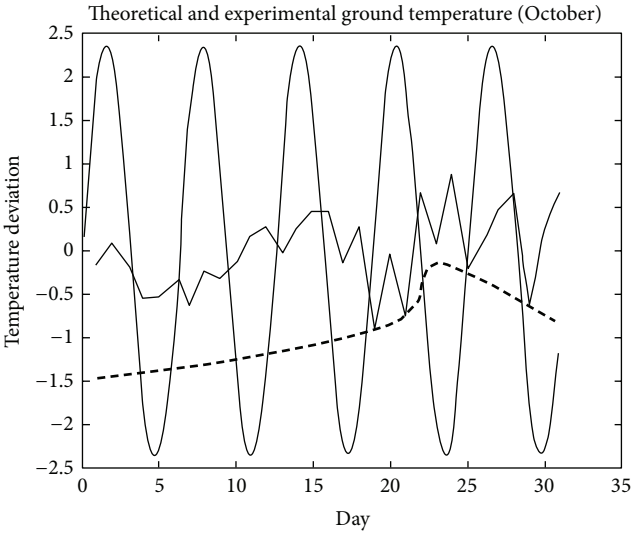

Figure 15: Theoretical and experimental combination for October.

of March (Figure 14). The solar radiation builds up after a major drop. The month of October, however, showed a nonlinear increase in solar radiation (as can be seen by the dotted lines) and a sudden drop (Figure 15). Practically, it is abnormal because this is the feature expected by December (ICDC, 2012).

In November, the abnormality of the solar radiation (evident from the ground temperature) spreads out (see Figure 16), despite following the same explanation like the previous month (October). December showed a decline in the solar radiation (see Figure 17).

In an explicit overview, the feature of December and January suggests that the solar radiation would follow the same trend in 2013. The undefined sequential formation for the months of January, February, October, November, and December suggests that the Kubwa region and by extension

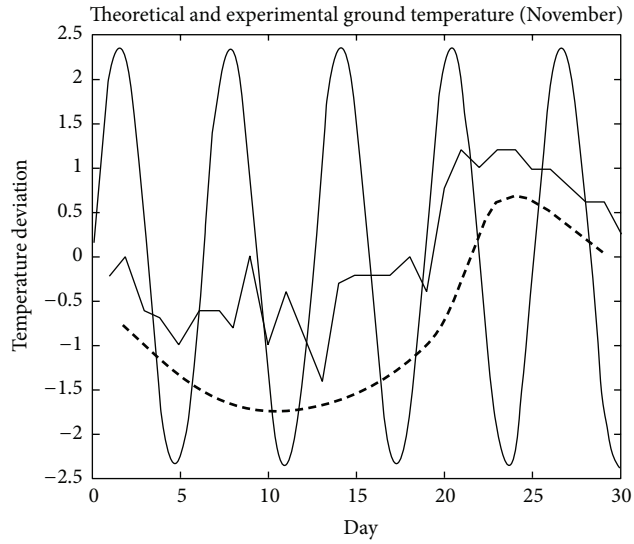

Figure 16: Theoretical and experimental combination for November.

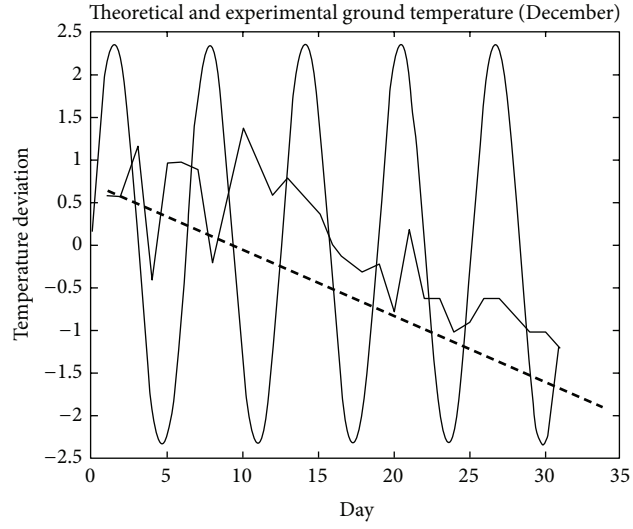

Figure 17: Theoretical and experimental combination for December.

to the north central region of Nigeria may experience a lower hydrological disaster in 2013 compared to the preceding year 2012. This assertion earlier reported by Uno et al. [9] had been confirmed by NASA imagery. This means that subsequent years may experience higher magnitude of flooding if the solar radiation is not balanced by the known climatic natural forces (air temperature, solar irradiance, precipitation patterns, Coriolis, pressure-gradient, and friction) and man-made alterations.

5. Conclusion

At shallow ground depth, the thermal diffusivity is not proportional to the increase or the decrease in the ground temperature. The abnormal shift of feature between October and December affirmed low flooding in the north central part of Nigeria in 2013. The repeated feature of October and November shows that there may be higher magnitudes of hydrological disaster years after. The satellite view (Figures 18 and 19) confirmed the validity of the ground survey. In Figure 18, the study site (shown by red dot) on both the satellite and geological map confirmed the rock formation and its advantage to the environmental thermographic model (ETM). Figure 19 shows almost the same temperature trend between ground and satellite graphs.

Therefore, the environmental thermographic model is an accurate tool to forecast hydrological disaster, that is, flooding. This method can be adopted in meteorological ground stations to investigate the net radiation over land.

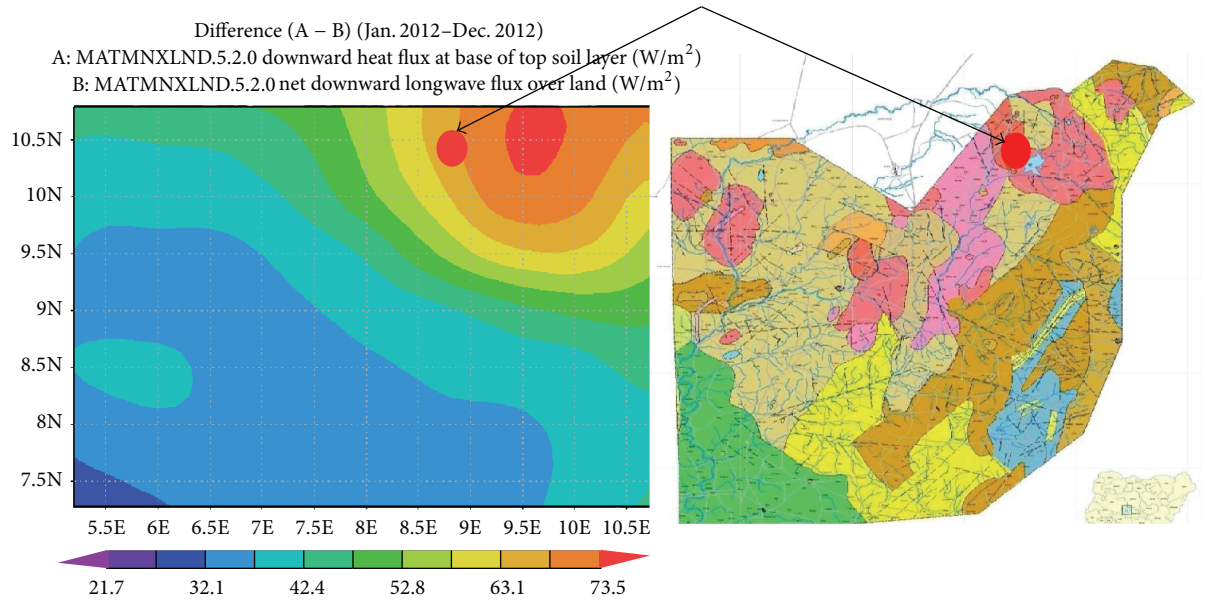

Figure 18: MERRA MATMNXLND.5.2.0 Satellite data over site (retrieved from NASA site).

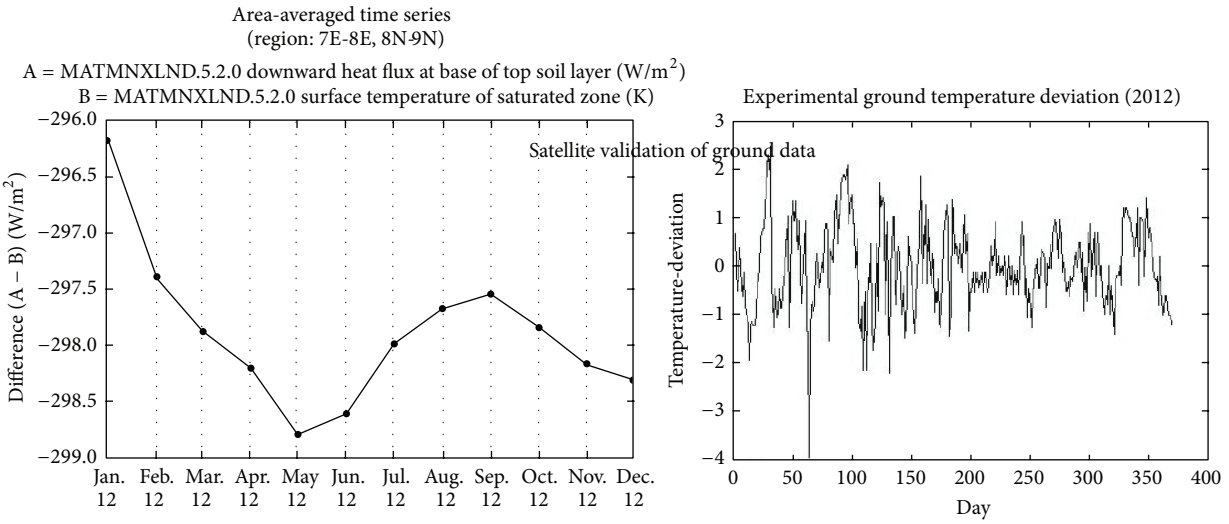

Figure 19: MERRA MATMNXLND.5.2.0 Satellite data over site (retrieved from NASA site).

The ability of the ETM could be extended to monitor ground anomalies like fractures of basic rocks amongst others.

Conflict of Interests

The author declares that there is no conflict of interests regarding the publication of this paper.

Acknowledgments

The author appreciates the Abuja Meteorological Agency and NASA for allowing him to compare their data. The author appreciates Covenant University for providing sponsorship of this research.

References

[1] B. R. Gardner, B. L. Blad, and G. D. Wilson, "Characterizing corn hybrid moisture stress sensitivity using canopy temperature measurements," *Remote Sensing of Environment*, vol. 19, no. 2, pp. 207–211, 1986.

[2] W. P. Kustas and K. S. Humes, "Spatially distributed sensible heat flux over a semiarid watershed. Part II: use of a variable resistance approach with radiometric surface temperatures," *Journal of Applied Meteorology*, vol. 36, no. 4, pp. 293–301, 1997.

[3] S. C. Gupta, J. K. Radke, and W. E. Larson, "Predicting temperatures of bare and residue covered soils with and without a corn crop," *Soil Science Society of America Journal*, vol. 45, no. 2, pp. 405–412, 1981.

[4] T. J. Toy, A. J. Kuhaida, and B. E. Munson, "The prediction of mean monthly soil temperature from mean monthly air temperature," *Soil Science*, vol. 126, no. 3, pp. 96–104, 1978.

[5] R. M. Cruse, D. R. Linden, J. K. Radke, and W. E. Larson, "A model to predict tillage effect on soil temperature," *Soil Science Society of America Journal*, vol. 44, pp. 378–383, 1980.

[6] R. J. Stathers, T. A. Black, and M. D. Novak, "Modelling soil temperature in forest clearcuts using climate station data," *Agricultural and Forest Meteorology*, vol. 36, no. 2, pp. 153–164, 1985.

[7] J. Goudriaan, "Simulation of micrometeorology of crops, some methods and their problems, and a few results," *Agricultural and Forest Meteorology*, vol. 47, no. 2–4, pp. 239–258, 1989.

[8] S. Marchenko, S. Hachem, V. Romanovsky, and C. Duguay, "Permafrost and active layer modeling in the Northern Eurasia using MODIS Land Surface Temperature as an input data," *Geophysical Research Abstracts*, vol. 11, p. 11077, 2009.

[9] U. E. Uno, M. E. Emetere, and U. U. Abdulrahman, "Parametric Analysis Of Ground Temperature Profile In Bwari-North Central Nigeria," *Journal of Environmental and Earth Science*, vol. 3, pp. 155–160, 2013.

[10] U. E. Uno and M. E. Emetere, "Analysing the impact of soil parameters on the sensible heat flux using simulated temperature curve model," *International Journal of Physics & Research*, vol. 2, no. 4, pp. 1–9, 2012.

[11] A. Mialon, A. Royer, M. Fily, and G. Picard, "Daily microwave-Derived surface temperature over Canada/Alaska," *Journal of Applied Meteorology and Climatology*, vol. 46, no. 5, pp. 591–604, 2007.

[12] J. C. Comiso, "Warming trends in the arctic from clear sky satellite observations," *Journal of Climate*, vol. 16, pp. 3498–3510, 2003.

[13] K. S. Humes, W. P. Kustas, and D. C. Goodrich, "Spatially distributed sensible heat flux over a semiarid watershed. Part I: use of radiometric surface temperatures and a spatially uniform resistance," *Journal of Applied Meteorology*, vol. 36, no. 4, pp. 281–292, 1997.

[14] T. Schmugge and S. J. Hook, "Recovering surface temperature and emissivity from thermal infrared data," in *Proceedings of the American Geophysical Union*, vol. F132, San Francisco, Calif, USA, 1995.

[15] K.-S. Han, A. A. Viau, and F. Anctil, "An analysis of GOES and NOAA derived land surface temperatures estimated over a boreal forest," *International Journal of Remote Sensing*, vol. 25, no. 21, pp. 4761–4780, 2004.

[16] Z. Wan and Z.-L. Li, "Radiance-based validation of the V5 MODIS land-surface temperature product," *International Journal of Remote Sensing*, vol. 29, no. 17-18, pp. 5373–5395, 2008.

[17] N. C. Coops, M. A. Wulder, and D. Iwanicka, "Large area monitoring with a MODIS-based disturbance index (DI) sensitive to annual and seasonal variations," *Remote Sensing of Environment*, vol. 113, no. 6, pp. 1250–1261, 2009.

[18] S. Westermann, M. Langer, and J. Boike, "Spatial and temporal variations of summer surface temperatures of high-arctic tundra on Svalbard—implications for MODIS LST based permafrost monitoring," *Remote Sensing of Environment*, vol. 115, no. 3, pp. 908–922, 2011.

[19] H. Beltrami, "Earth's long-term memory," *Science*, vol. 297, no. 5579, pp. 206–207, 2002.

[20] H. Beltrami and D. S. Chapman, "Drilling for a past climate," *New Science*, vol. 142, pp. 36–40, 1994.

[21] D. Hillel, *Introduction to Soil Physics*, Academic Press, San Diego, Calif, USA, 1982.

[22] U. E. Uno, M. E. Emetere, and J. S. Adelabu, "Parametric investigation of soil susceptibility to compaction using temperature deviation curves," *Journal of Civil Engineering and Architecture*, vol. 2012, no. 2, pp. 1–6, 2012.

[23] U. E. Uno, M. E. Emetere, and E. C. Daniel, "Simulated analysis of soil heat flux using temperature deviation curve model," *Science Journal of Physics*, vol. 2012, no. 2, pp. 1–9, 2012.

[24] M. E. Emetere, "Monitoring and prediction of earthquakes using simulated temperature deviation curve model," *International Journal of Applied Information Systems*, vol. 4, pp. 13–17, 2012.